GEOPHYSICS, VOL. 86, NO. 4 (JULY-AUGUST 2021); P. T229–T238, 6 FIGS.
10.1190/GEO2020-0682.1

A numerically exact nonreflecting boundary condition applied to the acoustic Helmholtz equation

Wim A. Mulder[1]

ABSTRACT

When modeling wave propagation, truncation of the computational domain to a manageable size requires nonreflecting boundaries. To construct such a boundary condition on one side of a rectangular domain for a finite-difference discretization of the acoustic wave equation in the frequency domain, the domain is extended on that one side to infinity. Constant extrapolation in the direction perpendicular to the boundary provides the material properties in the exterior. Domain decomposition can split the enlarged domain into the original one and its exterior. Because the boundary-value problem for the latter is translation-invariant, the boundary Green functions obey a quadratic matrix equation. Selection of the solvent that corresponds to the outgoing waves provides the input for the remaining problem in the interior. The result is a numerically exact nonreflecting boundary condition on one side of the domain. When two nonreflecting sides have a common corner, the translation invariance is lost. Treating each side independently in combination with a classic absorbing condition in the other direction restores the translation invariance and enables application of the method at the expense of numerical exactness. Solving the quadratic matrix equation with Newton's method turns out to be more costly than solving the Helmholtz equation and may select unwanted incoming waves. A proposed direct method has a much lower cost and selects the correct branch. A test on a 2D acoustic marine seismic problem with a free surface at the top, a classic second-order Higdon condition at the bottom, and numerically exact boundaries at the two lateral sides demonstrates the capability of the method. Numerically exact boundaries on each side, each computed independently with a free-surface or Higdon condition, provide even better results.

INTRODUCTION

Simulation of wave propagation in the earth often requires truncation to a subset of interest, except in global seismology when modeling the whole planet. Other applications involve infinite or very large domains that have to be reduced in size to keep the computations tractable. The required artificial boundaries should let outgoing waves pass without generating reflections. In practice, this turns out to be difficult, as witnessed by the large number of publications on the subject. Various reviews and comparison studies have appeared over time (Mittra et al., 1989; Mulder, 1997; Tsynkov, 1998; Tourrette and Halpern, 2001; Givoli, 2004; Hagstrom and Lau, 2007; Bérenger, 2015; Antoine et al., 2017; Gao et al., 2017).

In most applications, popular local and approximate schemes such as those by Engquist and Majda (1977) and Higdon (1986) and various types of perfectly matched layers (PMLs) (Bérenger, 1994; Chew and Weedon, 1994; Komatitsch and Martin, 2007) perform satisfactorily. In more demanding settings, for instance, in modeling seismic interbed multiples, conditions that perform better or that do not require tuning of parameters may be preferable. In those cases, exact nonreflecting boundary conditions are an option. An example is the method of Ting and Miksis (1986), which is based on Green's second identity. Because of a long-term instability, some dissipation has to be added (Givoli and Cohen, 1995). A reformulation as a boundary integral problem (Falletta and Monegato, 2014) does not require extra dissipation.

A step further are *numerically* exact nonreflecting boundary conditions (Ryaben'kii et al., 2001; Sofronov et al., 2015; Mulder, 2020a) that are exact for the *discretized* partial differential equation(s). A definition for the time domain is: "There is no difference

Manuscript received by the Editor 14 September 2020; revised manuscript received 10 March 2021; published ahead of production 23 April 2021; published online 08 July 2021.
[1]Shell Global Solutions International B.V., Amsterdam, The Netherlands and Delft University of Technology, Faculty of Civil Engineering and Geosciences, Department of Geoscience and Engineering, Delft, The Netherlands. E-mail: wim.mulder@shell.com (corresponding author).

DOI:10.1190/geo2020-0682.1

between a computation on the truncated domain with this method and one on an enlarged domain with reflecting boundaries that are placed so far away that their reflections cannot reach the original domain within the modeled time span" (Mulder, 2020a). That paper presents an improvement of the method of Sofronov et al. (2015) by using recursion to compute the elementary kernels, or the boundary Green functions as they will be called in this paper. This significantly improves the efficiency of the method. In spite of that, its convolutional character makes the approach still costly compared with existing approximate methods.

The goal of the current paper is to evaluate whether performing the calculations in the frequency domain instead of the time domain would help to further reduce cost. In the frequency domain, enlarging the domain may not help to remove the influence of the boundaries — unless the solution decays with distance. Adding some attenuation to the problem helps to accomplish that, especially in 1D, in which there is no geometric spreading that causes amplitude decay with distance.

The numerically exact nonreflecting boundary conditions for a finite-difference scheme on a rectangular domain use the discrete boundary Green functions, which are the responses in the extended part of the domain to Kronecker deltas on the boundary of the original domain. If the material properties outside the original domain are determined by constant extrapolation in the direction perpendicular to the boundary, the boundary Green functions can be computed by applying recursion and solving a wave equation in a small strip just outside the domain and parallel to the boundary.

Because the method assumes translation invariance perpendicular to the boundary, it can only be used if two numerically exact nonreflecting boundaries do not meet at a corner. This limits its applicability to cases in which open boundaries occur at opposing ends of the domain. One way to circumvent the corner problem is the application of a classic nonreflecting condition in the other coordinate direction (Mulder, 2020b). In the present paper, the classic second-order Higdon (1986, 1987) condition is chosen.

The next section describes the finite-difference discretization, the numerically exact boundary condition in one space dimension, its generalization to the 2D case, how to solve the quadratic matrix equation, and why a further generalization to 2.5D modeling is a problem. For the sake of exposition and as a proof of principle, the paper focuses on a second-order finite-difference approximation of the 2D frequency-domain acoustic wave equation. Higher order schemes are feasible (Mulder, 2020a), but they are not considered here. A 2D seismic marine example serves as a test problem for the method. A convergence study on a homogeneous problem provides accuracy and cost estimates.

METHOD

Discretization

The acoustic wave equation is adopted for seismic simulations as a simplification of the elastodynamic equations by setting the shear velocity to zero. In the frequency domain on a spatial domain Ω, it reads

$$-\frac{\omega^2}{\rho c^2}p-\nabla\cdot\left(\frac{1}{\rho}\nabla p\right)=s,\quad \text{in } \Omega, \tag{1}$$

where the pressure $p(\omega,\mathbf{x})$ depends on the angular frequency ω and position $\mathbf{x}\in\Omega$, $\rho(\mathbf{x})$ is the density, $c(\mathbf{x})$ is the sound speed, and $s(\omega,\mathbf{x})$ is a forcing function or source term, typically a delta function in seismic applications. In the presence of attenuation, the complex sound speed also depends on frequency (e.g., Aki and Richards, 2002):

$$\frac{1}{c(\omega,\mathbf{x})}=\frac{1}{c_0(\mathbf{x})}\left[1-\frac{1}{\pi Q}\log\left(\frac{\omega}{2\pi f_{\text{ref}}}\right)+\frac{\mathrm{i}}{2Q}\right], \tag{2}$$

where $Q(\mathbf{x})$ is the quality factor and the logarithmic term with reference frequency f_{ref}, typically 1 Hz, accounts for causality. In the following, the complex wavenumber is defined by $k(\omega,\mathbf{x})=\omega/c(\omega,\mathbf{x})$.

Equation 1 should be augmented with suitable boundary conditions, usually consisting in a zero Dirichlet condition at the surface Γ_0 of the earth or, in marine applications, of the water. At the rest of the boundary $\Gamma_n=\partial\Omega\setminus\Gamma_0$, nonreflecting boundaries of the form $\mathbf{n}\cdot\nabla p=Bp$ are imposed, where $\mathbf{n}$ denotes the normal to Γ_n and B represents the Dirichlet-to-Neumann map (Keller and Givoli, 1989; Deakin and Dryden, 1995).

A grid for a finite-difference discretization on a domain $\Omega=\{(x,z)|x\in[x_{\min},x_{\max}],z\in[z_{\min},z_{\max}]\}$ is defined by $x_i=x_{\min}+(i-1/2)\Delta x$ for $i=1,\ldots,N_x$ with a spacing $\Delta x=(x_{\max}-x_{\min})/N_x$, and likewise in the z-direction with $z_j=z_{\min}+(j-1/2)\Delta z$ for $j=1,\ldots,N_z$ and a spacing $\Delta z=(z_{\max}-z_{\min})/N_z$. With the lowest-order finite-difference scheme in 2D, this leads to

$$-k_{i,j}^2p_{i,j}-\frac{\rho_{i,j}}{\Delta x^2}\left[\frac{p_{i+1,j}-p_{i,j}}{\rho_{i+1/2,j}}-\frac{p_{i,j}-p_{i-1,j}}{\rho_{i-1/2,j}}\right]-\frac{\rho_{i,j}}{\Delta z^2}\left[\frac{p_{i,j+1}-p_{i,j}}{\rho_{i,j+1/2}}-\frac{p_{i,j}-p_{i,j-1}}{\rho_{i,j-1/2}}\right]=\rho_{i,j}s_{i,j}. \tag{3}$$

The average densities can be determined by $\rho_{i+1/2,j}=1/2(\rho_{i,j}+\rho_{i+1,j})$ and similarly for the other averages (Kummer et al., 1987; Moczo et al., 2002; Vishnevsky et al., 2014). Outside the computational domain, the material properties are assumed to be defined by constant extrapolation in the direction perpendicular to the boundary. If this is done one coordinate at the time, corner regions are automatically handled.

Before considering the numerically exact nonreflecting boundary condition in 2D, various boundary conditions will be discussed for the 1D case.

Boundary conditions in one dimension

Consider the boundary at $x_{\max}$ in the 1D case. A zero Dirichlet boundary condition is defined by setting $p_{N+1}=-p_N$, where N_x has been replaced by N. With the opposite sign, $p_{N+1}=p_N$, a zero Neumann boundary condition is imposed. The Sommerfeld radiation condition (Sommerfeld, 1964) at this boundary on the right sets $\mathrm{d}p/\mathrm{d}x=\mathrm{i}kp$ and lets waves of the form $e^{\mathrm{i}(kx-\omega t)}$ pass through from the interior to the exterior, where t denotes the time. If discretized by a first-order scheme, $(p_{N+1}-p_N)/\Delta x=\mathrm{i}kp_N$, resulting in $p_{N+1}=p_N(1+\mathrm{i}k\Delta x)$. With a second-order scheme, $(p_{N+1}-p_N)/\Delta x=\mathrm{i}k(p_{N+1}+p_N)/2$, providing

$$p_{N+1}=b(k_N)p_N,\quad b(k)=\frac{1+\mathrm{i}k\Delta x/2}{1-\mathrm{i}k\Delta x/2}. \tag{4}$$

This form of the Sommerfeld radiation condition agrees with the lowest order Enquist and Majda (1977) or Higdon (1986) condition. An exact version would be $p_{N+1}=p_N\exp(\mathrm{i}k\Delta x)$.

DOI:10.1190/geo2020-0682.1

A *numerically* exact boundary condition can be based on domain decomposition. Consider two domains Ω_1 and Ω_2. The first $\Omega_1 = [x_{\min}, x_{\max}]$ represents the original one. The second $\Omega_2 = [x_{\max}, \infty)$ is the exterior domain stretching to infinity. The boundary condition at $x_{\min}$ is, for instance, zero Dirichlet or Neumann, whereas only outgoing waves are allowed at $x \to \infty$, or, in the presence of attenuation, the solution should vanish at infinity. With these boundary conditions, the discrete problem on $\Omega_1 \cup \Omega_2$ can be expressed as

$$\begin{pmatrix} \mathbf{L}_{11} & \mathbf{L}_{12} \\ \mathbf{L}_{21} & \mathbf{L}_{22} \end{pmatrix} \begin{pmatrix} \mathbf{p}^{(1)} \\ \mathbf{p}^{(2)} \end{pmatrix} = \begin{pmatrix} \mathbf{s} \\ \mathbf{0} \end{pmatrix}. \tag{5}$$

The vector $\mathbf{p}^{(1)}$ contains the solution $(p_1, p_2, \ldots, p_N)^T$. The vector $\mathbf{p}^{(2)} = (p_{N+1}, p_{N+2}, \ldots)^T$ with exterior values is infinitely long. The discrete source term is represented by $\mathbf{s}$. The matrix $\mathbf{L}_{11}$ corresponds to the original problem on Ω_1, and $\mathbf{L}_{12}$ describes how the solution $\mathbf{p}^{(1)}$ on Ω_1 is affected by the solution values of $\mathbf{p}^{(2)}$ in the exterior domain Ω_2. With a second-order discretization, this only involves p_{N+1}. The infinite matrix $\mathbf{L}_{22}$ corresponds to the exterior Ω_2 and $\mathbf{L}_{21}$ describes how the solution $\mathbf{p}^{(2)}$ on Ω_2 depends on the interior solution $\mathbf{p}^{(1)}$. With a second-order discretization, this only involves p_N. Given the latter, the formal solution can expressed as

$$\mathbf{p}^{(2)} = -\mathbf{L}_{22}^{-1}\mathbf{L}_{21}\ p_N \quad = \mathbf{G}p_N\ , \tag{6}$$

where $\mathbf{G}$ is the boundary Green function, the response in the exterior of a unit spike on the boundary of the original domain. In the 1D case, it is a row vector of infinite length with elements G_k that correspond to the solution $p_{N+k} = G_k p_N$, $k > 0$, evaluated at $x_{N+k} = x_{\max} + (k - 1/2)\Delta x$, given the same grid definition as in the previous section. How to compute $\mathbf{G}$ is the central point of this paper, but before turning to the details, let us assume that it is known. The first block of rows in equation 5 then becomes

$$\mathbf{L}_{11}\mathbf{p}^{(1)} + \mathbf{L}_{12}G_1 p_N = \tilde{\mathbf{L}}\mathbf{p}^{(1)} = \mathbf{s}. \tag{7}$$

With a second-order finite-difference scheme in 1D, $\tilde{\mathbf{L}}$ is a tridiagonal matrix and can be solved with a direct method.

Next, the solution method for the boundary Green function $\mathbf{G}$ will be presented. If the material properties on Ω_2 are obtained by constant extrapolation from their values at $x_{\max}$, i.e., $c(x) = c(x_{\max})$ and $\rho(x) = \rho(x_{\max})$ for $x > x_{\max}$, the second row of blocks in equation 5 becomes

$$-k^2 p_i - \frac{1}{\Delta x^2}(p_{i+1} - 2p_i + p_{i-1}) = 0, \quad i > N. \tag{8}$$

Here, the complex wavenumber $k = k(x_{\max})$. With the ansatz $p_i = g^{i-N}p_N$, $i > N$, i.e., $G_i = g^{i-N}$, the second row of equation 5 becomes

$$-\frac{1}{\Delta x^2}(k^2\Delta x^2 + g - 2 + 1/g)\, g^{i-N}p_N = 0, \quad i > N. \tag{9}$$

The resulting quadratic equation in g has two solutions:

$$g = 1 - \frac{1}{2}(k\Delta x)^2 \pm \mathrm{i}(k\Delta x)^2\sqrt{1 - \frac{1}{4}(k\Delta x)^2}. \tag{10}$$

One corresponds to an incoming and one to an outgoing wave. The plus sign selects the outgoing wave. The solution g is the frequency-domain equivalent of the discrete boundary Green function of Mulder (2020a) or the elementary kernels of Sofronov et al. (2015). The result matches the earlier lowest-order Enquist-Majda or Higdon condition up to second order. The number of points per wavelength $n_\lambda = \lambda/\Delta x = 2\pi/(k\Delta x)$ should be $O(10)$ for sufficient accuracy with a second-order spatial discretization. In that case and in the absence of damping, the square root is real-valued.

Appendix A provides an alternative derivation in which the exact solution is adjusted to contain the discretization error, which is required if one wants a numerically exact boundary condition instead of an exact one for the underlying partial differential equation.

With the boundary condition of equation 10, there is no difference between the numerical solution on the domain $[x_{\min}, x_{\max}]$ and one on a much larger domain, other than numerical rounding errors, at least if there is some attenuation that causes the 1D solution to decay with distance.

The 2D case

For the generalization to 2D, we assume for the moment that all boundaries are reflecting, that is, zero Dirichlet or Neumann, and only the one on the right, at $x = x_{\max}$, is nonreflecting. Domain decomposition as shown in equation 5 now involves the enlarged domain $\Omega_1 \cup \Omega_2$, consisting of the original domain $\Omega_1 = \{(x, z)|x \in [x_{\min}, x_{\max}], z \in [z_{\min}, z_{\max}]\}$ and enlarged with $\Omega_2 = \{(x, z)|x \in [x_{\max}, \infty), z \in [z_{\min}, z_{\max}]\}$. The boundary conditions for Ω_2 at $z_{\min}$ and $z_{\max}$ should be the same as those for Ω_1, whereas at $x \to \infty$, only outgoing waves are allowed or, in the presence of attenuation, the solution should vanish at infinity. The material properties, which are the sound speed, density, and quality factor in the acoustic case, are obtained in Ω_2 by constant extrapolation in the direction perpendicular to the boundary $\Omega_1 \cap \Omega_2$ at $x = x_{\max}$. Because of that, the block tridiagonal operator $\mathbf{L}_{22}$ is translation-invariant in the x-direction, resulting in

$$\begin{aligned} &-k_{N_x,j}^2\Delta x^2 p_{i,j} - (p_{i+1,j} - 2p_{i,j} + p_{i-1,j}) \\ &-\frac{\Delta x^2}{\Delta z^2}\rho_{N_x,j}\left[\frac{p_{i,j+1} - p_{i,j}}{\rho_{N_x,j+1/2}} - \frac{p_{i,j} - p_{i,j-1}}{\rho_{N_x,j-1/2}}\right] = 0, \\ &\quad i > N_x, j = 1, \ldots, N_z. \end{aligned} \tag{11}$$

The boundary condition at $z_{\min}$ is imposed by $p_{i,0} = \pm p_{i,1}$, with the minus sign for a Dirichlet or the plus sign for a Neumann boundary condition, and the boundary condition at $z_{\max}$ is imposed by $p_{i,N_z+1} = \pm p_{i,N_z}$. For fixed i, equation 11 can be expressed as

$$(\mathbf{A}\mathbf{p}_{[i]})_j - p_{i+1,j} - p_{i-1,j} = 0, \quad i > N_x, j = 1, \ldots, N_z, \tag{12}$$

where $\mathbf{p}_{[i]}$ is a vector with the solution values $p_{[i],j} = p_{i,j}$ and $\mathbf{A}$ is a tridiagonal $N_z \times N_z$ matrix containing the terms corresponding to $p_{i,j}$, $p_{i,j-1}$, and $p_{i,j+1}$ in equation 11. Because of the translation invariance, $\mathbf{A}$ does not depend on i.

To solve the boundary-value problem on Ω_2 after domain decomposition, we start with $p_{N_x,j}$ from Ω_1 in equation 11 and make the ansatz that $\mathbf{p}_{[i]} = \mathbf{G}^{i-N_x}\mathbf{p}_{[N_x]}$, $i > N_x$, where $\mathbf{G}$ now is an $N_z \times N_z$ matrix that only describes the response in the set of exterior points neighboring the boundary and not in all exterior points as in the 1D case. Substitution into equation 12 provides

DOI:10.1190/geo2020-0682.1

$$\mathbf{AG}-\mathbf{G}^2-\mathbf{I}=\mathbf{0}, \quad i=N_x+1, \tag{13a}$$

$$(\mathbf{AG}-\mathbf{G}^2-\mathbf{I})\mathbf{G}^{i-1-N_x}=\mathbf{0}, \quad i>N_x+1, \tag{13b}$$

where $\mathbf{I}$ is the $N_z \times N_z$ identity matrix. Because $\mathbf{G}$ may be singular, the case with $i=N_x+1$ is listed separately.

Equations 13a and 13b can be satisfied by solving the quadratic matrix equation 13a. Its solutions are called solvents (Dennis et al., 1987; Higham and Kim, 2000; Tisseur and Meerbergen, 2001). The related quadratic eigenvalue problem has $2N_z$ eigenvalues, which can be split into two sets (Higham and Kim, 2000). The largest N_z eigenvalues correspond to a solvent that is called dominant, and the smallest N_z correspond to a solvent that is called minimal. For the wave equation with nonzero attenuation, the outgoing waves have decaying amplitudes and should vanish at $x \to \infty$, so the minimal and not the dominant solvent is needed. Details will be given next.

The resulting matrix $\mathbf{G}$ contains the boundary Green function $G_{i,j;N_x,j_0}$ at $i=N_x+1$, defined as the response in the point $(x_i,z_j) \in \Omega^{(2)}$ for a unit solution value at the point $(x_{N_x},z_{j_0}) \in \Omega^{(1)}$ and zero in all other $(x_{N_x},z_j) \in \Omega^{(1)}$ for $j \neq j_0$. The solution in the domain Ω_2, corresponding to the second part of the domain-decomposition problem in equation 5 but then generalized to 2D, is given by

$$p^{(2)}_{i,j}=\sum_{j_0=1}^{N_z}\left(G^{i-N_x}\right)_{j;j_0} p^{(1)}_{N_x,j_0}, \quad i>N_x, j=1,\ldots,N_z. \tag{14}$$

The superscripts (1) and (2) are redundant but are still included to emphasize in which domain the solution resides. The remaining part in Ω_1 of the domain-decomposition problem becomes

$$\mathbf{L}_{11}\,\mathbf{p}^{(1)}+\mathbf{L}_{12}\,\mathbf{G}\mathbf{p}^{(1)}_{[N_x]}=\tilde{\mathbf{L}}\mathbf{p}^{(1)}=\mathbf{s}, \tag{15}$$

representing the acoustic wave equation in Ω_1 with a numerically exact boundary condition at $x=x_{\max}$. This 2D problem with matrix $\tilde{\mathbf{L}}$ is still amenable to a direct sparse-matrix solver, although the occurrence of $\mathbf{G}$ causes a loss of sparsity on the boundary.

If nonreflecting boundaries meet at a corner, translation invariance breaks down and it is not clear how to determine the boundary Green functions in an efficient manner. To avoid this problem, an alternative approach is the independent treatment of each boundary separately. Instead of the zero Dirichlet or Neumann boundary condition at $z_{\min}$ and $z_{\max}$, as assumed above, we can impose a classic nonreflecting boundary condition such as those of Sommerfeld (1964), Engquist and Majda (1979), Higdon (1986, 1987), or Bérenger (1994). In the frequency domain, the PML of the latter is nothing but a complex coordinate stretching (Chew et al., 1997).

Here, I will use the classic second-order boundary condition of Higdon (1986, 1987). The main reason is that it preserves the sparsity pattern of the discrete Helmholtz operator and that it is easy to implement. The last is also true for a PML, but that condition requires an additional strip of grid points.

The second-order Higdon boundary condition at $z_{\max}$ in the time domain reads

$$\left[\prod_{m=1}^{2}\left(\frac{\partial}{\partial t}+c_m\frac{\partial}{\partial z}\right)\right]p=0, \tag{16}$$

where $c_m=c_b/\cos\theta_m$ and c_b is the sound speed at the boundary. Equation 16 lets incoming waves at angles θ_m, $m=1,2$ pass without reflections. In the subsequent example, the chosen angles are $\theta_1=0°$ and $\theta_2=60°$. Define the shift operator T_z by $T_z p_{i,j}=p_{i,j+1}$. A discrete form of equation 16 in the frequency domain is

$$\left[\prod_{m=1}^{2}\left(-\mathrm{i}k_m\frac{T_z+1}{2}+\frac{T_z-1}{\Delta z}\right)\right]T_z^{-1}p_{i,N_z}=0, \tag{17}$$

where $k_m=\omega/c_m$. With $b_m=b(k_m)$ as defined in equation 4, this simplifies to

$$p_{i,N_z+1}=(b_1+b_2)p_{i,N_z}-b_1b_2p_{i,N_z-1}. \tag{18}$$

This expression for the extrapolated value enables the elimination of p_{i,N_z+1} in terms of p_{i,N_z} and p_{i,N_z-1} from the Helmholtz operator in equation 3 as well as equations 11 and 12. The resulting expression for $\mathbf{A}$ will differ from the one for a Dirichlet or Neumann boundary condition at $z_{\max}$; hence, equation 15 will lead to a different boundary matrix $\mathbf{G}$ and operator $\tilde{\mathbf{L}}$.

A nonreflecting boundary condition at $x_{\min}$ follows from a similar approach, with its own matrix $\mathbf{A}$, similar to equation 12 but with $i<1$, providing another boundary Green function $\mathbf{G}$. A further step is the use of the boundary Green functions on each side of the original domain independently, including $z_{\max}$ and, in the absence of a free surface, $z_{\min}$. In this way, the Higdon boundary conditions only appear in each matrix $\mathbf{A}$ that corresponds to a 1D problem on a line just outside and parallel to one side of the domain. As a result, the Higdon conditions are no longer explicitly present in the modified Helmholtz operator $\tilde{\mathbf{L}}$, but only implicitly via the boundary Green functions.

Because the resulting boundary Green functions $\mathbf{G}$ are decoupled by treating them independently for each side of the domain, the net result is different from the true boundary Green function for the entire boundary consisting of all the nonreflecting sides taken together. The latter provides a truly numerically exact nonreflecting boundary condition, but an affordable numerical method for its computation has not yet been found for problems in which the model parameters are not constant in the exterior.

Quadratic matrix equation

An obvious choice for the solution of the quadratic matrix equation 13a is Newton's method. To reduce the risk of convergence toward an incorrect solution, $\mathbf{G}$ is initialized as a diagonal matrix with the 1D result with the plus sign in equation 10 for each j. Newton's method requires the Jacobian of the nonlinear problem, which is a sparse matrix of size $N_z^2 \times N_z^2$. Initially, it contains N_z copies of $\mathbf{A}$, so about $3N_z$ nonzero entries, but after a few iterations that increases to $O(N_z^3)$ nonzero entries. More precisely, it fills up to N_z square block diagonals, each of size $N_z \times N_z$, and N_z off-diagonals, each a horizontal or vertical distance N_z apart, resulting in slightly less than $2N_z^3$ nonzero entries. This is usually much larger than the almost $5N_xN_z$ nonzero entries of the interior operator $\mathbf{L}_{11}$. The cost of solving for the Jacobian matrix in several iterations, typically approximately 8 to reach 10^{-15}, rapidly exceeds that of solving the interior Helmholtz problem if the number of grid points increases. Although the resulting boundary Green function can be reused for multiple problems as long as the grid points and wavenumbers on

the boundary at $x_{\max}$ do not change, this does not make the method attractive.

Another iterative method, equation 26 of Higham and Kim (2000), in the current setting reads

$$\mathbf{I} - \mathbf{A}\mathbf{G}^{(m+1)} + \mathbf{G}^{(m)}\mathbf{G}^{(m+1)} = \mathbf{0}, \tag{19}$$

where the iteration count m starts at $\mathbf{G}^{(0)} = \mathbf{0}$ and becomes

$$\mathbf{G}^{(0)} = \mathbf{0}, \quad \mathbf{G}^{(m+1)} = (\mathbf{A} - \mathbf{G}^{(m)})^{-1}, \quad m \geq 0. \tag{20}$$

This fixed-point iteration provides the minimal solvent, as required for outgoing waves. The repeated matrix inversions are still costly, given the fact that $\mathbf{G}^{(m)}$ becomes a full matrix.

A more robust and efficient approach uses the eigenvalues and eigenvectors of $\mathbf{A}$. Because $\mathbf{A}$ is tridiagonal, although not complex symmetric and not Hermitian, its eigenvalues and eigenvectors can be computed at a relatively low compute cost. Let $\mathbf{Q}$ be the matrix with the eigenvectors as columns and $\Lambda = \mathbf{Q}^{-1}\mathbf{A}\mathbf{Q}$ a diagonal matrix with the corresponding eigenvalues of $\mathbf{A}$. The quadratic matrix equation can be transformed to

$$\mathbf{0} = \mathbf{Q}^{-1}[\mathbf{G}^2 - \mathbf{A}\mathbf{G} + \mathbf{I}]\mathbf{Q} = \Gamma^2 - \Lambda\Gamma + \mathbf{I}, \quad \Gamma = \mathbf{Q}^{-1}\mathbf{G}\mathbf{Q}. \tag{21}$$

The solution of this set of N_z equations is the diagonal matrix Γ with elements

$$\gamma_{j,j} = (\lambda_{j,j}/2) + \mathrm{i}\sqrt{1 - (\lambda_{j,j}/2)^2}, \quad j = 1, \ldots, N_z, \tag{22}$$

where $\lambda_{j,j}$ are the diagonal elements of Λ. This procedure avoids the risk of selecting the incorrect branch. The boundary Green functions for each of the boundary points are the columns of

$$\mathbf{G} = \mathbf{Q}\Gamma\mathbf{Q}^{-1}. \tag{23}$$

With this approach, the cost of finding $\mathbf{G}$ is of the same order but lower than that of solving the Helmholtz equation 3 with any of the classic boundary conditions. In addition, the boundary condition based on $\mathbf{G}$ changes the original Helmholtz operator $\mathbf{L}_{11}$ in equation 16. The resulting operator $\tilde{\mathbf{L}}$ has a different sparsity pattern with a full instead of a sparse matrix on the boundary, which increases the cost of solving the interior problem.

2.5D

An interesting generalization of the method is the 3D problem with model parameters that are constant in the y-direction. Let $\mathbf{L}^{(2D)}$ represents the earlier 2D operator in the (x, z)-plane at $y = 0$. A grid in y with spacing Δy is defined by $y_\ell = \ell\Delta y$ for integer $\ell \in [-\infty, \infty]$. The 3D operator at $y = 0$ or $\ell = 0$ has additional off-diagonals $-1/\Delta y^2$ at $\ell = -1$ and $\ell = 1$ and an extra $2/\Delta y^2$ on its main diagonal. Define $\mathbf{A} = \Delta y^2\mathbf{L}^{(2D)} + 2\mathbf{I}$ as the subset of the 3D operator acting on solution values at $\ell = 0$ and multiplied by Δy^2. Here, the identity operator $\mathbf{I}$ has the same size as the 2D operator $\mathbf{L}^{(2D)}$, the latter equipped with classic nonreflecting boundary conditions. With this scaling, the off-diagonals in y become $-\mathbf{I}$ and the boundary Green function $\mathbf{G}$ for the y-direction obeys $\mathbf{A}\mathbf{G} - \mathbf{G}^2 - \mathbf{I} = \mathbf{0}$, as previously, but it now predicts solution values at $\ell = 1$ from those at $\ell = 0$.

Using mirror symmetry in the y-direction, the Helmholtz equation in 3D at $y = 0$ becomes $\mathbf{A}\mathbf{u} - 2\mathbf{G}\mathbf{u} = \Delta y^2\mathbf{s}'$, with $s'_{i,0,j} = \rho_{i,j}\, s_{i,0,j}$ defined as the source term at (x_i, y_0, z_j) with the density included. If the matrix $\mathbf{Q}$ contains the eigenvectors of $\mathbf{A}$ and the diagonal matrix Λ the corresponding eigenvalues, the quadratic eigenvalue can be solved in the same way as previously and Helmholtz's equation has the solution $\mathbf{u} = \mathbf{Q}\mathbf{M}\mathbf{Q}^{-1}\Delta y^2\mathbf{s}'$, where the diagonal matrix $\mathbf{M}$ has entries $\mu_{j,j} = 1/(\lambda_{j,j} - 2\gamma_{j,j})$, $j = 1, \ldots, N_x N_z$. Choosing a spacing Δy smaller than Δx and Δz will help to reduce the size of the discretization error in the y-direction.

Although this extension to 2.5D requires little additional coding and looks deceptively simple, the eigenvalue and eigenvector computation makes it too costly to be of practical use, unfortunately. A better choice is a spatial Fourier transform in the y-direction with repeated computations of the 2D Helmholtz problems (Zhou and Greenhalgh, 1998; Novais and Santos, 2005; Xiong et al., 2011).

EXAMPLES

Inhomogeneous problem

Figure 1a displays the sound speed, $c_0(\mathbf{x})$ in equation 2, and Figure 1b shows the density, $\rho(\mathbf{x})$, for a marine example with a salt

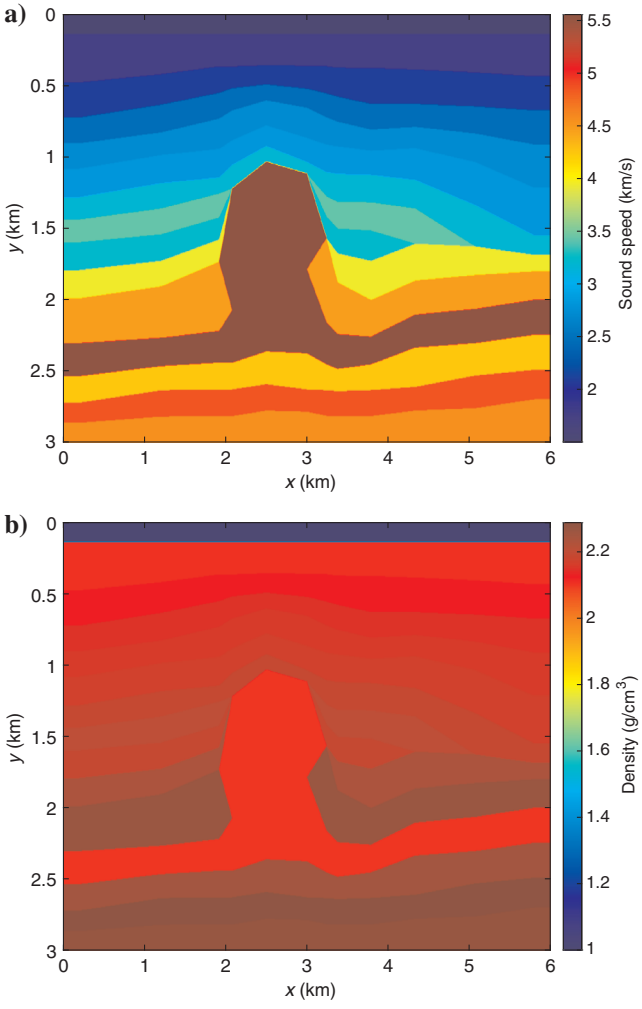

Figure 1. (a) Velocity model and (b) density.

diapir. Here, z increases with depth. The model consists of a water layer just below the free surface at the top, at $z = 0$, followed by sediment layers. The salt diapir has a high sound speed but lower density. Close to the boundaries at the left and right, the layers are flattened to avoid diffractions when the model is extended in the direction perpendicular to the boundary by constant extrapolation. The proposed method can only work if the medium is translation-invariant in the direction perpendicular to the boundary. Dipped layers on the boundary require a transition region toward a model with that property, perhaps with smoothed contrasts.

The finite-difference grid has a spacing of 5 m, resulting in 1200×600 points. The quality factor for attenuation was set to 10^{10} in the water layer and to 100 elsewhere. A nonzero value for $1/Q$ is generally advised to stabilize the solution of Helmholtz's equation, which is close to indefinite.

A point source located at (502.5, 7.5) m generated the wavefield shown in Figure 2 for a frequency of 24 Hz. The source amplitude was set to $1/(\Delta x \Delta z)$ to mimic a delta function. Note that the amplitude range for the real part is larger than for the imaginary part and both have been reduced to 20% of their maximum to bring out the weaker parts of the signal. To assess the performance of the boundary conditions, a reference solution was computed on a larger domain, using the earlier classic second-order Higdon boundary conditions combined with a rather thick PML layer (Bérenger, 1994; Chew and Weedon, 1994) in the part outside the original domain. Figure 2a and 2b was actually obtained from a subset of that solution.

Figure 3 shows the difference between the wavefield obtained with the second-order Higdon boundary conditions at the left, right, and bottom, and the reference solution. In this case, the full amplitude range is shown. Because the source is located near the left boundary, its reflections are strongest. With the numerically exact boundary conditions at the left and right, combined with the classic condition at the bottom, the results of Figure 4a and 4b are obtained. These only show reflections from the bottom, which are much smaller than those from the sides as is evident from the much larger amplitudes in Figure 3. Finally, Figure 5 combines the numerically exact boundary conditions at the left and right with the same at the bottom, but with a free-surface condition at $z_{\min} = 0$. The second-order Higdon boundary conditions

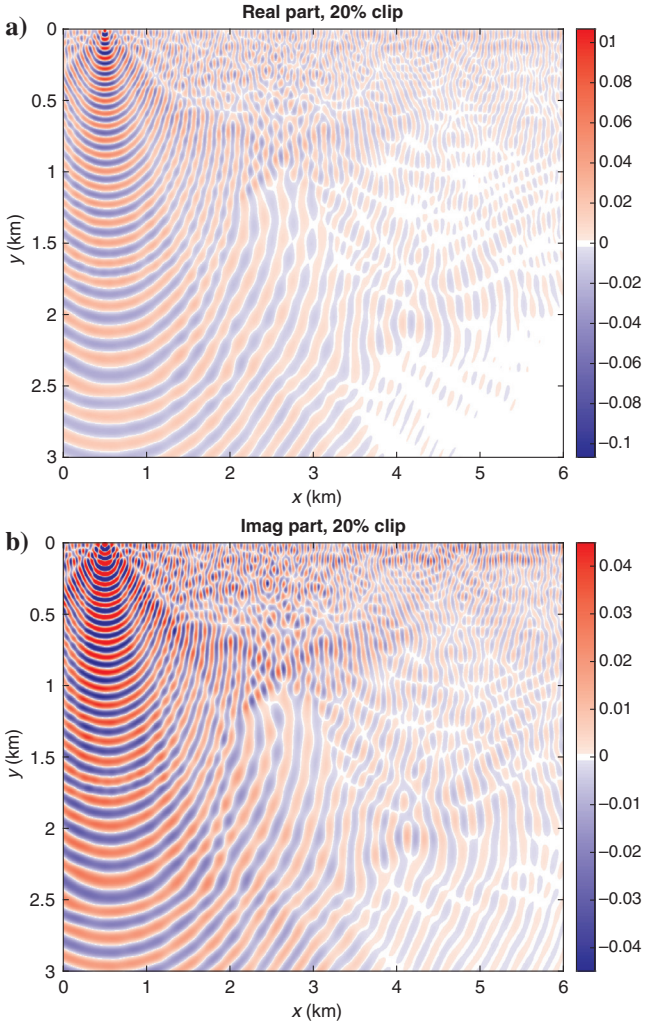

Figure 2. (a) Real and (b) imaginary part of the reference solution, each clipped at 20% of its maximum amplitude.

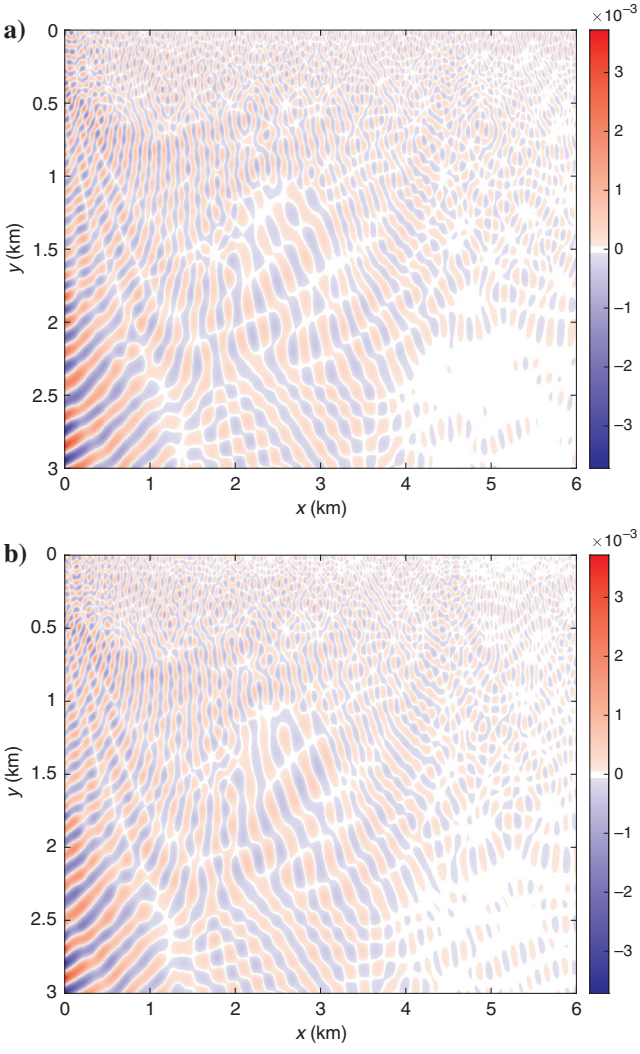

Figure 3. (a) Real and (b) imaginary part of the difference between a solution computed with the second-order Higdon boundary conditions and the reference solution.

now only enter at the endpoints in the 1D problems for computation of the boundary Green functions on each side. The resulting difference with the reference solution is smaller than the one in Figure 4, except at the bottom-left corner. Note that Figures 4a, 4b, 5a, and 5b were all plotted with the same amplitude scale. Reflections from the two corners at the bottom remain because waves that travel around the corner were ignored in the computation of the boundary Green functions.

Homogeneous problem

The reference solution in the previous example was a very accurate approximation to the numerical solution with the same grid spacing on an infinite half-space because the goal was to examine how close the proposed method could come to a truly numerically exact nonreflecting boundary condition. In the current example, the reference solution is the exact one of a homogeneous problem with a free-surface boundary condition at zero depth. The difference between the numerical solution and the reference solution will then consist of the combined effect of the discretization error and the deviation for the numerically exact boundary condition.

The domain is 1.0 km wide and 0.4 km deep, the sound speed c is 1 km/s, and the density is 2 g/cm^3. A point source is placed at a grid point nearest to $x_s = 400$ m and $z_s = 100$ m. Its amplitude is $1/(\Delta x \Delta z)$, as in the previous example. The frequency is 20 Hz, and the wavenumber $k = (\omega/c)(1 + 10^{-5}\mathrm{i})$. The small imaginary part helps to avoid numerical instabilities on fine grids.

The proposed boundary condition will be compared with the second-order Higdon and a PML boundary condition. The last had the simplest quadratic form of complex stretching (Collino and Tsogka, 2001; Zhang and Shen, 2010). In the x-direction with a strip of width $L_x = N_{\mathrm{PML}}\Delta x$ at the right boundary, at $x_{\max}$, this leads to a stretched coordinate $\tilde{x}$ defined by

$$\mathrm{d}\tilde{x} = \left(1 - \frac{d(x)}{\mathrm{i}\omega}\right)\mathrm{d}x, \quad d(x) = d_0\left(\frac{x - x_{\max}}{L_x}\right)^2. \tag{24}$$

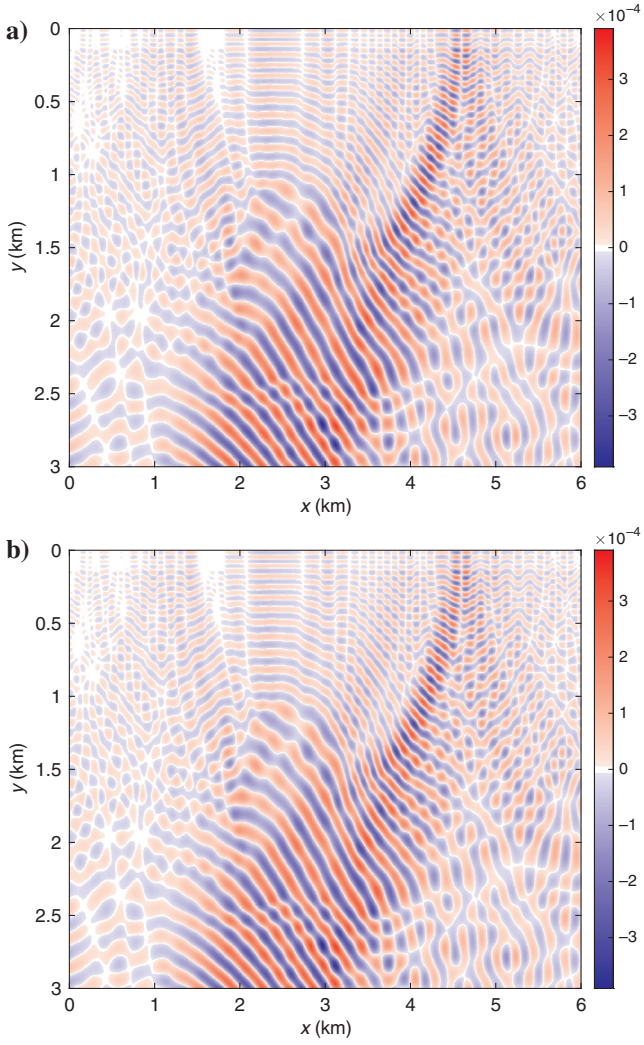

Figure 4. (a) Real and (b) imaginary part of the difference between a solution computed with the numerically exact boundary conditions at the left and right and the second-order Higdon boundary condition at the bottom and the reference solution.

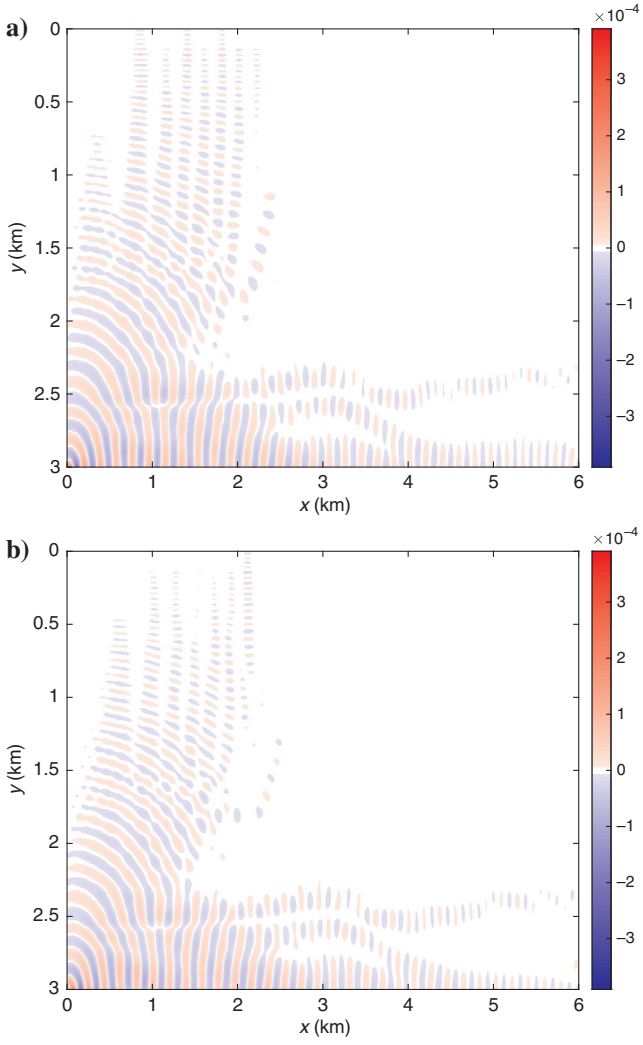

Figure 5. (a) Real and (b) imaginary parts of the difference between a solution computed with the numerically exact boundary conditions independently at the left, right, and bottom and the reference solution.

The minus sign accounts for the opposite sign convention. The PML layer ends at $x_{\max} + L_x$ with a zero Dirichlet boundary condition. Collino and Tsogka (2001) suggest a parameter

$$d_0 = -\frac{3}{2}\frac{c}{L_x}\beta_0 \log(R_0), \tag{25}$$

with $\beta_0 = 1$ for the 1D case. In the current example, the choice of parameters is $N_{\text{PML}} = 20$, $R_0 = 10^{-4}$, and $\beta_0 = 2$.

Figure 6a compares the relative root-mean-square (rms) error of the solution as a function of the grid spacing $\Delta x = \Delta z$. The rms error is taken as the square root of the summed squared absolute values of the errors on the interior domain, divided by the summed squared absolute values of the exact solution, excluding the values at the source position where the solution is singular. The error behaves as $O(\Delta x^2)$ for the larger grid spacings in this test, consistent with the approximation error of the finite-difference discretization, but it flattens out on finer grids because of the boundary reflections. With the second-order Higdon condition applied to the sides and bottom, this already happens on fairly coarse grids. With the proposed scheme, applying the numerically exact conditions independently along each side, the unwanted reflected waves start to dominate the error only on much finer grids.

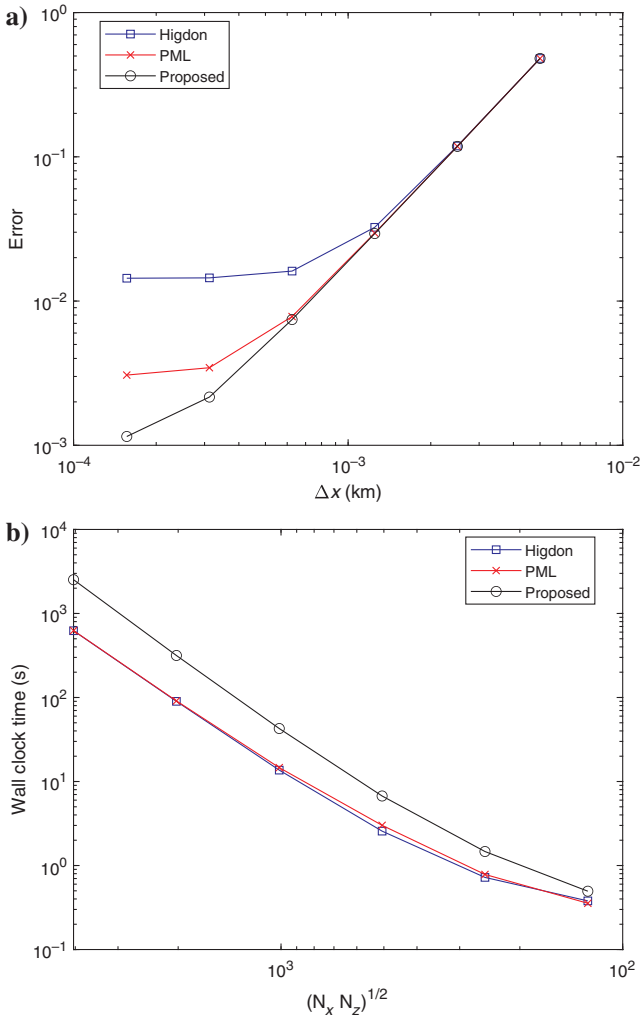

Figure 6. (a) Relative rms error as a function of the grid spacing $\Delta x = \Delta z$ for a homogeneous problem. Convergence with the second-order Higdon condition levels off at a much larger value of Δx than with the proposed method, which maintains second-order accuracy to much finer grids, whereas the PML condition with the chosen parameters ends up in between. (b) Measured wall clock time as a function of the square root of the number of grid points. The horizontal axis has its direction reversed to follow (a).

This comes at a cost. Figure 6b shows the observed wall clock time as a function of $(N_x N_z)^{1/2}$ with N_x being the number of grid points in the x-direction and N_z in the z-direction. The horizontal axis is reversed to follow Figure 6a. The computations were carried out in MATLAB [version 9.6.0 (R2019a)] with only a single thread. On the finer grids, the elapsed wall-clock time scales roughly as $(N_x N_z)^{2.5}$ with the Higdon condition and as $(N_x N_z)^{2.7}$ with the proposed approach. The higher cost is due to solving the quadratic matrix equation three times, once per side of the domain, and to the loss of sparsity at the boundaries, which increases the cost of solving the Helmholtz problem. The Higdon condition is less costly than the PML, but on finer grids, the difference becomes smaller because the number of extra points for the PML conditions is kept constant. The proposed method is 1.4–4.0 times more costly in this example.

DISCUSSION

Numerically exact nonreflecting boundary conditions have a considerable computational cost in the time domain. The present study shows that, in the frequency domain, the additional cost in 2D is roughly of the same order as that of solving the Helmholtz equation, making these boundary conditions a viable option.

Still, the computation of the boundary Green functions and the loss of sparsity at the boundary of the discrete Helmholtz operator make the method more expensive than the local Higdon or PML boundary conditions. Note that the boundary Green functions can be reused if the model parameters at the boundary and the grid stay the same, thereby allowing for a further cost reduction. Nevertheless, a PML boundary condition can reach the same accuracy at a lower cost after careful tuning. The proposed method has the advantage that it is simple to code and does not require extensive tuning.

When modeling multiple shots or running a full-waveform inversion, the frequency-domain formulation is more efficient than the time domain for 2D problems (Marfurt and Shin, 1989; Štekl and Pratt, 1998; Mulder and Plessix, 2002). In 3D, that is no longer true because computation of the boundary Green functions becomes too expensive.

CONCLUSIONS

Numerically exact nonreflecting boundary conditions in the time domain have a substantial computational cost even with the use of recursion. In the frequency domain with a finite-difference discretization of the 2D acoustic wave equation on a rectangular domain, computation of the eigenvalues and eigenvectors of a 1D Helmholtz equation can bring down the cost to the same order as that of solving the 2D Helmholtz equation in the interior.

The current approach considers each nonreflecting side of the rectangular domain separately. After extending the domain from one side to infinity, domain decomposition splits the enlarged domain into the original one and its extension. In the latter, constant extrapolation in the direction perpendicular to the boundary can

provide the material properties such as the sound speed, density, and quality factor in the acoustic case. As a result, the discrete operator in the exterior is translation-invariant. The boundary Green functions then follow from a quadratic matrix equation. Its solution with Newton's method has an associated computational cost that quickly exceeds that of solving the Helmholtz equation in the interior. In addition, there is the risk of selecting incoming instead of outgoing waves. Instead, we can compute the eigenvalues and eigenvectors of a 1D Helmholtz equation and explicitly choose the outgoing wave. With that approach, the computational cost becomes acceptable.

The boundary Green functions only depend on the material properties next to the boundary. Therefore, they can be reused for other problems as long as the grid and the properties on the boundary remain the same.

Treating each side independently causes a loss of exactness when two nonreflecting boundaries meet at a corner. With a classic boundary condition applied in the other coordinate direction, the method becomes only partially exact but remains useful, as a 2D acoustic example representing a marine seismic problem demonstrates.

DATA AND MATERIALS AVAILABILITY

Data sharing is not applicable to this article as no new data were created or analyzed in this study. However, if the computational results shown in the figures are considered as new data, then the author elects not to share those.

APPENDIX A

ALTERNATIVE DERIVATION IN 1D

As mentioned for the 1D case, an exact boundary condition at $x_{\max}$ would let $p_{N+1} = p_N \exp(\mathrm{i}k\Delta x)$, but this expression is not numerically exact. For the latter, we have to reinsert the discretization error. If the solution is of the form $g = e^{\mathrm{i}\kappa\Delta x}$, then the discrete partial differential equation (PDE) lets $(g - 2 + g^{-1})/\Delta x^2 = -k^2$, providing $4\sin^2(\kappa\Delta x/2) = (k\Delta x)^2$ or $\sin(\kappa\Delta x/2) = k\Delta x/2$. This means that the discrete PDE models the 1D Helmholtz equation exactly, but at a different wavenumber $k = \kappa\,\mathrm{sinc}(\kappa\Delta x/2)$, where $\mathrm{sinc}(x) = \sin(x)/x$. Then,

$$\begin{aligned} g = e^{\mathrm{i}\kappa\Delta x} &= e^{\pm 2\,\mathrm{i}\arcsin\left(\frac{1}{2}k\Delta x\right)} \\ &= 1 - \frac{1}{2}(k\Delta x)^2 \pm \mathrm{i}(k\Delta x)\sqrt{1 - \frac{1}{4}(k\Delta x)^2}, \end{aligned} \tag{A-1}$$

which is the same as equation 10. The branch with $+\mathrm{i}$ provides a wave traveling to the right. Its series expansion is $g = 1 + \mathrm{i}(k\Delta x) - 1/2(k\Delta x)^2 + O((k\Delta x)^3)$ and agrees with the Sommerfeld or lowest order Enquist-Majda or Higdon condition up to the second-order term.

REFERENCES

Aki, K., and P. G. Richards, 2002, Quantitative seismology, 2nd ed.: University Science Books.

Antoine, X., E. Lorin, and Q. Tang, 2017, A friendly review of absorbing boundary conditions and perfectly matched layers for classical and relativistic quantum waves equations: Molecular Physics, **115**, 1861–1879, doi: 10.1080/00268976.2017.1290834.

Bérenger, J.-P., 1994, A perfectly matched layer for the absorption of electromagnetic waves: Journal of Computational Physics, **114**, 185–200, doi: 10.1006/jcph.1994.1159.

Bérenger, J.-P., 2015, A historical review of the absorbing boundary conditions for electromagnetics: Forum for Electromagnetic Research and Application Technologies, **9**, 1–28, https://www.e-fermat.org/files/articles/154db8c5adee49.pdf.

Chew, W. C., J. M. Jin, and E. Michielssen, 1997, Complex coordinate stretching as a generalized absorbing boundary condition: Microwave and Optical Technology Letters, **15**, 363–369, doi: 10.1002/(SICI)1098-2760(19970820)15:6<363::AID-MOP8>3.0.CO;2-C.

Chew, W. C., and W. H. Weedon, 1994, A 3D perfectly matched medium from modified Maxwell's equations with stretched coordinates: Microwave and Optical Technology Letters, **7**, 599–604, doi: 10.1002/mop.4650071304.

Collino, F., and C. Tsogka, 2001, Application of the perfectly matched absorbing layer model to the linear elastodynamic problem in anisotropic heterogeneous media: Geophysics, **66**, 294–307, doi: 10.1190/1.1444908.

Deakin, A., and J. Dryden, 1995, Numerically derived boundary conditions on artificial boundaries: Journal of Computational and Applied Mathematics, **58**, 1–16, doi: 10.1016/0377-0427(93)E0261-J.

Dennis, J. E., J. F. Traub, and R. P. Weber, 1987, Algorithms for solvents of matrix polynomials: SIAM Journal on Numerical Analysis, **15**, 523–533, doi: 10.1137/0715034.

Engquist, B., and A. Majda, 1977, Absorbing boundary conditions for the numerical simulation of waves: Mathematics of Computation, **31**, 629–629, doi: 10.1090/S0025-5718-1977-0436612-4.

Engquist, B., and A. Majda, 1979, Radiation boundary conditions for acoustic and elastic wave calculations: Communications on Pure and Applied Mathematics, **32**, 313–357, doi: 10.1002/cpa.3160320303.

Falletta, S., and G. Monegato, 2014, An exact non reflecting boundary condition for 2D time-dependent wave equation problems: Wave Motion, **51**, 168–192, doi: 10.1016/j.wavemoti.2013.06.001.

Gao, Y., H. Song, J. Zhang, and Z. Yao, 2017, Comparison of artificial absorbing boundaries for acoustic wave equation modelling: Exploration Geophysics, **48**, 76–93, doi: 10.1071/EG15068.

Givoli, D., 2004, High-order local non-reflecting boundary conditions: A review: Wave Motion, **39**, 319–326, doi: 10.1016/j.wavemoti.2003.12.004.

Givoli, D., and D. Cohen, 1995, Nonreflecting boundary conditions based on Kirchhoff-type formulae: Journal of Computational Physics, **117**, 102–113, doi: 10.1006/jcph.1995.1048.

Hagstrom, T., and S. Lau, 2007, Radiation boundary conditions for Maxwell's equations: A review of accurate time-domain formulations: Journal of Computational Mathematics, **25**, 305–336.

Higdon, R. L., 1986, Absorbing boundary conditions for difference approximations to the multi-dimensional wave equation: Mathematics of Computation, **47**, 437–459, doi: 10.2307/2008166.

Higdon, R. L., 1987, Numerical absorbing boundary conditions for the wave equation: Mathematics of Computation, **49**, 65–65, doi: 10.1090/S0025-5718-1987-0890254-1.

Higham, N. J., and H.-M. Kim, 2000, Numerical analysis of a quadratic matrix equation: IMA Journal of Numerical Analysis, **20**, 499–519, doi: 10.1093/imanum/20.4.499.

Keller, J. B., and D. Givoli, 1989, Exact non-reflecting boundary conditions: Journal of Computational Physics, **82**, 172–192, doi: 10.1016/0021-9991(89)90041-7.

Komatitsch, D., and R. Martin, 2007, An unsplit convolutional perfectly matched layer improved at grazing incidence for the seismic wave equation: Geophysics, **72**, no. 5, SM155–SM167, doi: 10.1190/1.2757586.

Kummer, B., A. Behle, and F. Dorau, 1987, Hybrid modeling of elastic-wave propagation in two-dimensional laterally inhomogeneous media: Geophysics, **52**, 765–771, doi: 10.1190/1.1442343.

Marfurt, K. J., and C. S. Shin, 1989, The future of iterative modeling in geophysical exploration, Chapter 9, *in* E. Eisner, ed., Supercomputers in seismic exploration: Pergamon, Handbook of Geophysical Exploration, **21**, 203–228, doi: 10.1016/B978-0-08-037018-7.50013-1.

Mittra, R., O. O. Ramahi, A. Khebir, R. Gordon, and A. Kouki, 1989, A review of absorbing boundary conditions for two and three-dimensional electromagnetic scattering problems: IEEE Transactions on Magnetics, **25**, 3034–3039, doi: 10.1109/20.34361.

Moczo, P., J. Kristek, V. Vavryčuk, R. J. Archuleta, and L. Halada, 2002, 3D heterogeneous staggered-grid finite-difference modeling of seismic motion with volume harmonic and arithmetic averaging of elastic moduli and densities: Bulletin of the Seismological Society of America, **92**, 3042–3066, doi: 10.1785/0120010167.

Mulder, W. A., 1997, Experiments with Higdon's absorbing boundary conditions for a number of wave equations: Computational Geosciences, **1**, 85–108, doi: 10.1023/A:1011556926362.

Mulder, W. A., 2020a, Exact non-reflecting boundary conditions with an FDTD scheme for the scalar wave equation in waveguide problems: Progress in Electromagnetics Research, **91**, 39–48, doi: 10.2528/PIERM19121202.

Mulder, W. A., 2020b, Research note: A workaround for the corner problem in numerically exact non-reflecting boundary conditions: Geophysical Prospecting, **68**, 2857–2866, doi: 10.1111/1365-2478.13018.
Mulder, W. A., and R.-É. Plessix, 2002, Time-versus frequency-domain modelling of seismic wave propagation: 64th Annual International Conference and Exhibition, EAGE, Extended Abstracts, E015, doi: 10.3997/2214-4609-pdb.5.E015.
Novais, A., and L. T. Santos, 2005, 2.5D finite-difference solution of the acoustic wave equation: Geophysical Prospecting, **53**, 523–531, doi: 10.1111/j.1365-2478.2005.00488.x.
Ryaben'kii, V. S., S. V. Tsynkov, and V. I. Turchaninov, 2001, Global discrete artificial boundary conditions for time-dependent wave propagation: Journal of Computational Physics, **174**, 712–758, doi: 10.1006/jcph.2001.6936.
Sofronov, I. L., L. Dovgilovich, and N. Krasnov, 2015, Application of transparent boundary conditions to high-order finite-difference schemes for the wave equation in waveguides: Applied Numerical Mathematics, **93**, 195–205, doi: 10.1016/j.apnum.2014.06.006.
Sommerfeld, A., 1964, Lectures on theoretical physics: Academic Press.
Štekl, I., and R. G. Pratt, 1998, Accurate viscoelastic modeling by frequency-domain finite differences using rotated operators: Geophysics, **63**, 1779–1794, doi: 10.1190/1.1444472.
Ting, L., and M. J. Miksis, 1986, Exact boundary conditions for scattering problems: The Journal of the Acoustical Society of America, **80**, 1825–1827, doi: 10.1121/1.394297.
Tisseur, F., and K. Meerbergen, 2001, The quadratic eigenvalue problem: SIAM Review, **43**, 235–286, doi: 10.1137/S0036144500381988.
Tourrette, L., and L. Halpern, 2001, Absorbing boundaries and layers, domain decomposition methods: Applications to large scale computers: Nova Science Publishers Inc.
Tsynkov, S. V., 1998, Numerical solution of problems on unbounded domains: A review: Applied Numerical Mathematics, **27**, 465–532, doi: 10.1016/S0168-9274(98)00025-7.
Vishnevsky, D., V. Lisitsa, V. Tcheverda, and G. Reshetova, 2014, Numerical study of the interface errors of finite-difference simulations of seismic waves: Geophysics, **79**, no. 4, T219–T232, doi: 10.1190/geo2013-0299.1.
Xiong, J., A. Abubakar, Y. Lin, and T. M. Habashy, 2011, 2.5D forward and inverse modeling of elastic full-waveform seismic data: 81st Annual International Meeting, SEG, Expanded Abstracts, 2395–2400, doi: 10.1190/1.3627690.
Zhang, W., and Y. Shen, 2010, Unsplit complex frequency-shifted PML implementation using auxiliary differential equations for seismic wave modeling: Geophysics, **75**, no. 4, T141–T154, doi: 10.1190/1.3463431.
Zhou, B., and S. A. Greenhalgh, 1998, Composite boundary-valued solution of the 2.5-D Green's function for arbitrary acoustic media: Geophysics, **63**, 1813–1823, doi: 10.1190/1.1444475.

A biography and photograph of the author are not available.